Chapter 1

Introduction

The first chapter provides a brief description about the Sun and its different layers both in its interior and exterior. Thereafter, we outline some basic information about the solar magnetism and the solar cycle. We describe the localized magnetic features on the Sun, and their linkage with a variety of transient activities. We provide a brief description of different transient phenomena (e.g., solar flares, eruptive prominences, large-scale coronal jets, coronal mass ejections (CMEs), etc). Since, the present thesis focuses on the study of coronal jets, we provide a focused review on the observational as well as theoretical developments to understanding the coronal jets. We also discuss their possible linkage with the CMEs. At the end, we briefly describe the outline of the various chapters of this thesis.

1.1 The Sun: An Overview

The Sun is the source of energy for the entire solar system and all aspects of our lives are directly impacted by what happens on the Sun. Also, the Sun's proximity makes it unique among the billions of stars in the sky of which we can resolve its surface features and study physical processes at work. Observations of the Sun's atmosphere led to the development

of the theory of radiative transfer in stellar atmospheres and the discovery of the element helium. The Sun is a giant magnetohydrodynamic (MHD) laboratory for large magnetic Reynolds numbers, which exhibit phenomena of magnetic fibrils, sunspots, prominences, flares, coronal loops, coronal jets, CMEs, the solar wind, the X-ray corona, and irradiance variations etc. The physics of these exotic phenomena collectively make up variations of solar activity. The solar activity affects the terrestrial environment, from occasionally knocking out power grids to space weather and most probably general climate.

Beginning with the first solar ultraviolet light from space in 1946, X-rays in 1948, hard X-rays and γ-rays in 1958; many experiments have been conducted or being conducted using balloons, rockets and satellites (e.g., OSOs (Bonnet *et al.*, 1978), Skylab (Gosling *et al.*, 1974), SMM (Bohlin *et al.*, 1980), Yohkoh (Acton *et al.*, 1992), SOHO (Domingo, Fleck and Poland, 1995), TRACE (Schrijver *et al.*, 1996), RHESSI (Lin *et al.*, 2004), Hinode (Kosugi *et al.*, 2007), STEREO (Driesman, Hynes and Cancro, 2008), SDO (Pesnell, Thompson and Chamberlin, 2012), Solar Orbiter (Müller *et al.*, 2020) etc.). Artificial satellites have provided the unique opportunity to conduct uninterrupted observations of the Sun from the vantage points, such as the Sun-Earth Lagrangian point L1 (e.g., SOHO), or from outside the ecliptic plane (e.g., Ulysses), or in stereoscopic modes using different orbits (e.g., STEREO). Lagrangian L1 is a Sun-Earth lagrangian point where the gravitational pull of Sun and Earth is equal to the centripetal force required by a spacecraft to move with them. L1 point is used by a spacecraft to remain in a fixed position and give an uninterrupted view of the Sun. Ground-based observations suffer from the effects of the Earth's atmosphere such as atmospheric extinction resulting in the limited radiative spectrum of the Sun, and turbulence resulting in image distortions. The Earth's outer atmosphere does not allow the pentration of the UV and X-rays to reach to the ground, so the solar corona and its transients events can not be observed through the ground-based observations. Therefore, it is required to explore the dynamics of the

Sun's corona using the space-borne UV/EUV and X-ray instruments and related imaging or spectroscopic observations. Making use of adaptive optics system, solar images with resolution of about 0.13 arc sec (90 km on the Sun), or even smaller structures down to 60 km, have been obtained by the Swedish 1-meter Solar Telescope (SST) at La Palma. With the advent of 4m-The Daniel K. Inouye Solar Telescope (DKIST) telescope at Hawaii this year, the current limit of resolution has gone down to 30 km at the Sun, and it will provide a scope to understand a variety of sub-arcsec dynamical plasma processes in the solar atmosphere revealing unprecedented information about a variety of long-standing problems in solar physics. Neutrino detectors have also provided a unique tool for probing the Sun's interior by comparing the emitted flux with the predictions of the standard solar models. Helioseismology from space and from ground (e.g., GONG) have revolutionized our understanding of the workings of the Sun. Helioseismology is a tool which describes the different properties of solar interior by using solar global modes oscillations. The uses of helioseismology are to study the solar interior, solar internal rotation and solar dynamo process. The Sun plays an important role to provide a suitable laboratory conditions to study different transient phenomena and a variety of physical processes in the solar interior as well as in the solar atmosphere. Its proximity allows close observations of its different surfaces and its study can provide deep understanding of behavior of cosmic plasma and other stars. It affects climate and space-weather conditions on the Earth. The Sun is a G2V type star which has 4.8 stellar magnitude with some of its typical basic properties (cf., Table 1.1). The spherically symmetric structure of the Sun is balanced by its gravity and plasma pressure (Golub and Pasachoff, 1997; Schrijver and Zwaan, 2000). Different physical properties of the Sun is given in Table 1.1.

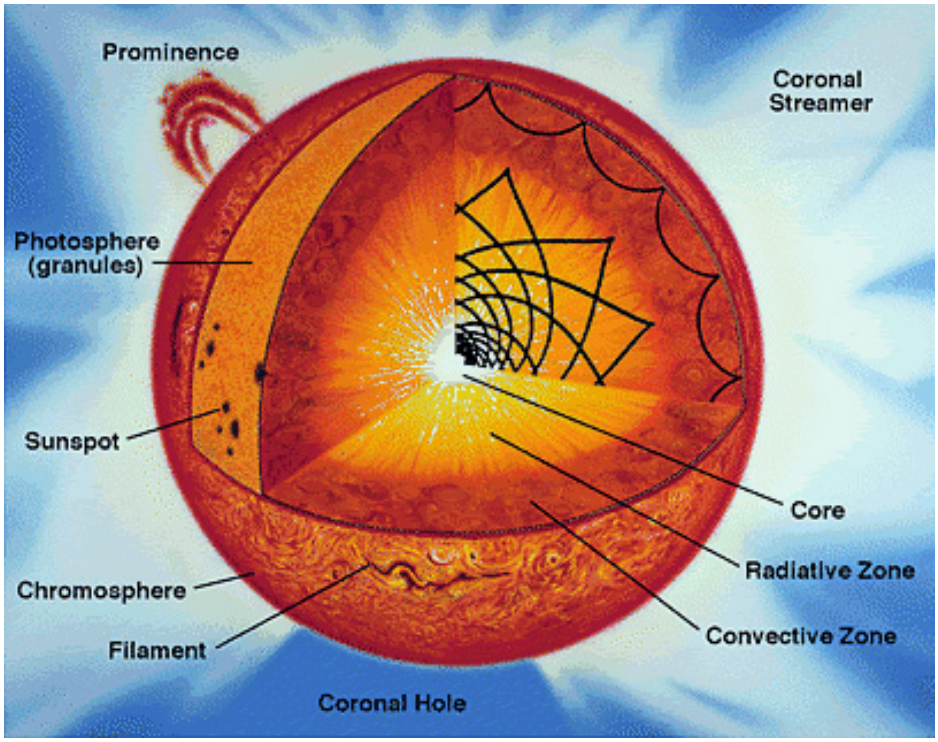

Figure 1.1: The structure of solar interior and exterior is displayed. A variety of magnetic structures are also shown in the various layers of the solar atmosphere from the photosphere to the corona.(Courtesy: http://eclipse99.nasa.gov/pages/SunActiv.html)

Table 1.1: The Sun's Physical Properties

S.No.	Physical Property	Value
i	Age	$4.6 \times 10^9 yr$
ii	Radius	$695.5 Mm$
iii	Surface Temperature	$5785 K$
iv	Mass	$1.99 \times 10^{30} kg$
v	Mass-loss rate	$10^9 kgs^{-1}$
vi	Luminosity	$3.86 \times 10^{26} W$
vii	Mean density	$1.4 \times 10^3 kgm^{-3}$
viii	Surface gravity	$274 ms^{-2}$
ix	Mean distance from the Earth	$1.496 \times 10^{11} m$
x	Escape velocity at the surface	$618 kms^{-1}$

1.2 Solar Interior

The structure of the Sun can be divided into two parts: solar interior and solar exterior. The Sun has well-defined regions (cf., Figure 1.1) much like the solid part of an Earth-like planet and its atmosphere. The solar radiation comes from nuclear reactions deep in the Sun's core. The energy leaks out, first by radiation and then by convection, until it reaches the visible surface, and escapes into space. Figure 1.1 shows different zones of solar interior and different layers of the solar atmosphere. The solar interior comprises with inner core, convective zone and radiative zone. The different physical processes signify different layers of the Sun's interior. The surface of the Sun is visible but its inner core is fully shielded which can be studied by means of helioseismology. The Sun contains different elements such as H (92 %) , He (8%) and C, N, O which contributes 0.1 % part of the Sun (Asplund *et al.*, 2009). The core of the Sun has high temperature (15×10^6 K) and high density (1.6×10^5 $kg\ m^{-3}$) which provides favourable conditions for thermo-nuclear fusion reactions in that region. Figure 1.2 shows the size, density and temperature parameters in different layers of the solar interior.

Inner Core

The Sun has gigantic nuclear reactor in its inner core which generates 99 % energy of the Sun. The energy is generated by nuclear fusion process. In the nuclear fusion process H nuclei fuses and forms He nuclei in which huge amount of energy releases (Q=26.73 MeV). The final product of PP and CNO cycle is ^4He. ^4He atom has less mass than the 4 protons. This mass loss is converted in excess energy by mass-energy equivalence. Here, the term Q represents the released energy in the nuclear fusion process. This fusion process can

take place by two different cycles as proton-proton (PP) cycle and carbon-nitrogen-oxygen (CNO) cycle (Priest, 2014). Proton-proton (PP) cycle generates ≈ 98 % solar energy while CNO cycle generates ≈ 2 % solar energy (Chitre, 2003).

The fusion reactions of PP cycle are written as;

$$p + p \rightarrow d + e^{+} + \nu_e \tag{1.1}$$

$$p + e^{-} + p \rightarrow d + \nu_e \tag{1.2}$$

$$p + d \rightarrow {}^{3}He + \gamma \tag{1.3}$$

When ${}^{3}He$ is formed there are some ways by which ${}^{3}He$ can be converted into ${}^{4}He$ e.g. PP-I, PP-II and PP-III branches. Here PP-I branch is mentioned;

$${}^{3}He + {}^{3}He \rightarrow {}^{4}He + 2p \tag{1.4}$$

$${}^{3}He + p \rightarrow {}^{4}He + e^{+} + \nu_e \tag{1.5}$$

The overall product of P-P chain is wriiten as;

$$4p \rightarrow {}^{4}He + 2e^{+} + 2\nu_e + Q \tag{1.6}$$

Now, the fusion reactions of CNO cycle are written as;

$${}^{12}C + p \rightarrow {}^{13}N + \gamma \tag{1.7}$$

$${}^{13}N \rightarrow {}^{13}C + e^{+} + \nu_e \tag{1.8}$$

$${}^{13}C + p \rightarrow {}^{14}N + \gamma \tag{1.9}$$

$${}^{14}N + p \rightarrow {}^{15}O + \gamma \tag{1.10}$$

$${}^{15}O \rightarrow {}^{15}N + e^{+} + \nu_e \tag{1.11}$$

$${}^{15}N + p \rightarrow {}^{12}C + {}^{4}He \tag{1.12}$$

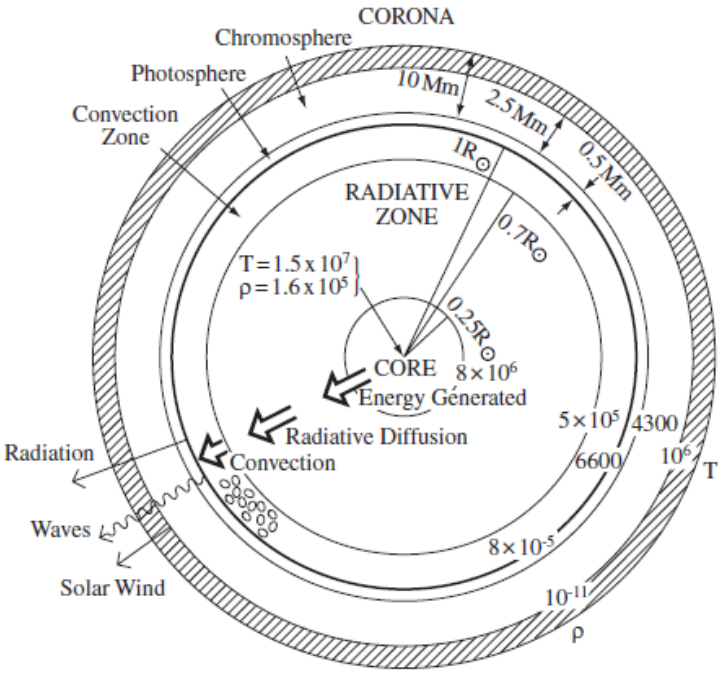

Figure 1.2: The size (in Mm), density (in kgm^{-3}) and temperature (in K) structuring in different regions of the Sun. (Courtesy: Priest (2014))

where p, e^-, e^+, ν_e, ^4He are respectively proton, electron, positron, electron neutrino and helium.

Radiative Zone

The radiative zone is located above the inner core of the Sun. This zone radiates whole energy which is generated in the inner core by radiation process. Photons in this zone interact with plasma particles and their absorption and emission happen frequently by which photons take much time to cross the radiative zone (Mitalas and Sills, 1992).

When we move outwards of the radiative zone, the opacity starts to increases by which temperature gradient also increases and convective instability (Schwarzhild Criterion) sets there and it becomes convective zone.

Convective Zone

This zone is located above the radiative zone and energy is transported by convection process in this zone. The Sun's large scale magnetic field is generated in tachocline

(sheared layer) at the lower surface of convective zone by dynamo process (Spiegel and Zahn, 1992). Tachocline is a sheared transition layer between two rotating regions i.e., radiative interior and outer convective zone which rotates differentially (Miesch, 2005). All solar magnetic fields do not come from tachocline layer. Strong azimuthal toroidal magnetic fields are produced in that sheared layer. The motion of hot plasma appears as granules pattern at the solar surface (Title *et al.*, 1989). According to Schwarzschild criterion the radial temperature gradient is greater than adiabatic temperature gradient in convection zone, so in this region energy transportation is possible by plasma motions only and there is no contribution of radiation process (Priest, 2014),

$$\mid \frac{dT}{dr} \mid > \mid \left(\frac{dT}{dr}\right)_{ad} \mid \tag{1.13}$$

where $\frac{dT}{dr}$, $(\frac{dT}{dr})_{ad}$ denote the radial temperature gradient and adiabatic temperature gradient respectively.

1.3 Solar Atmosphere

The lowest layer of the solar exterior is known as "The Solar Photosphere". Above the photosphere, it is the Sun's tenuous atmosphere. The chromosphere is the lowest part which is visible as a thin bright red crescent during total eclipses. Beyond the chromosphere, it is the pearly white corona, extending out to many times the radius of the photosphere ($\approx$700,000 km). Further out still, the corona consists of a stream of charged particles known as the solar wind, pervading the entire solar system. Different layers of solar atmosphere are briefly described as follows and displayed in Figure 1.1:

Photosphere

The solar photosphere is considered as a visible surface layer of the Sun. It is a few hundred km wide and emits most of the solar visible radiations in the form of a black-body. Its temperature ranges from 4500 to 6000 K with an average value lying around 5800

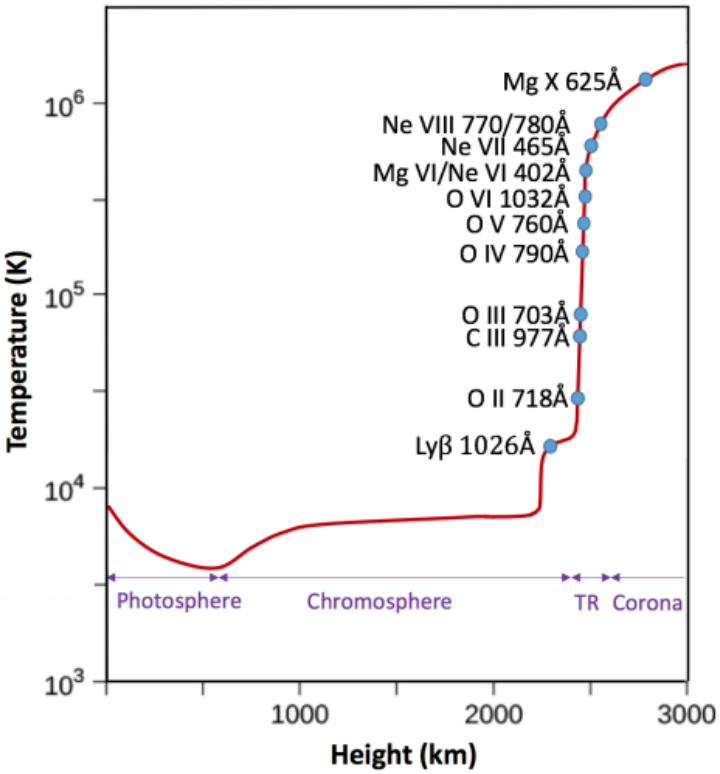

Figure 1.3: The variation of temperature with solar height above solar photosphere. Different ion lines as per their formation temperature are also indicated in the image. (Courtesy: Tian (2017))

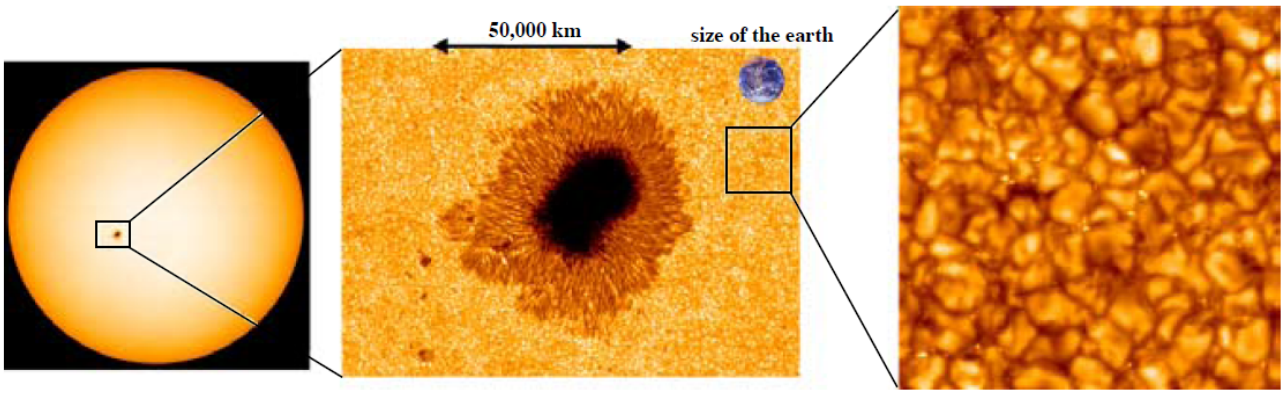

Figure 1.4: Image of the solar photosphere and its magnetic regions, i.e., quiet-Sun granules, and active region sunspot. (Courtesy: Hinode, S. Tsuneta)

K. It has an average density of 3×10^{-7}gm.cm^{-3}. Figure 1.3 shows temperature variation in different layers of the solar atmosphere, where it is clearly seen that photospheric temperature is maintained at around 5800 K. Solar photosphere releases radiative energy (Solanki, 1998). The top level of convection zone is visible in this layer in the form of granulation and super-granulation patterns (cf., Figure 1.4). The convective flows work as an active perturbation in driving of the p-mode (3 mHz or 5 min) oscillations (Frazier, 1966). The convective flows (i.e., granulation process) work as an active agent/perturbationsin driving p-modes (5-min) oscillations in the photosphere.

As mentioned above, the observational manifestation of the convection in upper part of solar interior is the appearance in 'quiet' photosphere as polygonal cells, roughly 1000 km across (1.5" in angular measure), lasting 15 minutes (largest granules last longer). In quiet photosphere, granules are 30% brighter than intergranular lanes – this translates to a temperature difference of 400 K. Very bright dots appear in intergranular lanes sometimes forming chains which trace out a network. This is governed by a large-scale supergranulation forming a larger-scale of the flow pattern and subsequently responsible for the generation of quiet-Sun magnetic field pattern extended even upto the solar chromosphere. By magnetic buoyancy and other related instabilities the generated magnetic field in tachocline region overshoots, rises in the convection zone and finally emerges at the solar surface as bipolar magnetic fields. The active regions at the photosphere consist of sunspots (cf., Figure 1.4). The dark sunspot is associated with strong magnetic field of the order of 1000 Gauss. Features on solar photosphere e.g., faculae, bright points, sunspots and magnetic pores represent high magnetic flux regions which play an important role in photospheric motions (Berger, Rouppe van der Voort and Löfdahl, 2007). Faculae are bright patches found at the side of granules. The bright appearance of faculae is due to less magnetic flux and transparency in that region (Keller *et al.*, 2004). The photospheric bright

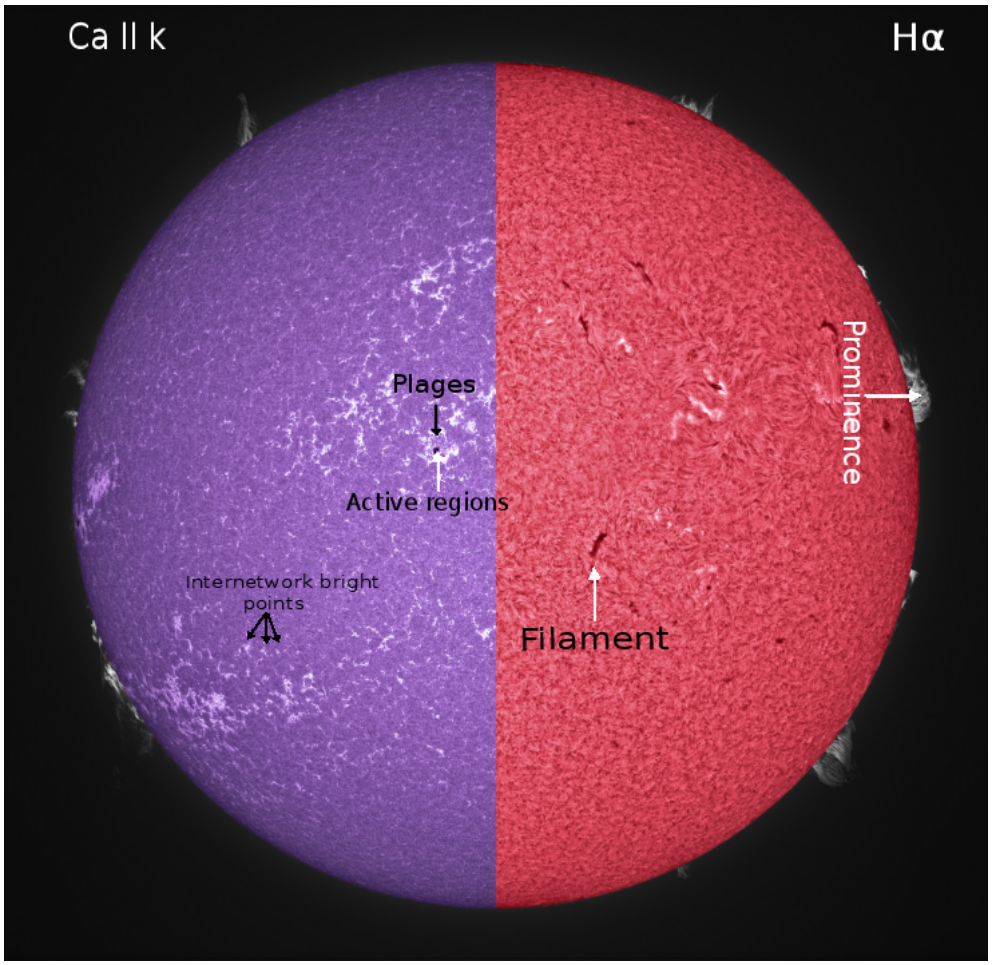

Figure 1.5: Image of the solar chromosphere and its various magnetic structures (Courtesy: Alan Friedman)

points are smaller in size as compared to faculae and generally found at supergranular boundaries in the quiet-Sun region.

In conclusion, the solar photosphere consists of a variety of magnetic structures at diverse spatial scales and their respective strength of the magnetic fields from few tens of Gauss to few thousand Gauss. It exhibits a range of dynamical phenomena, plasma motions and related processes, and radiative emissions.

Chromosphere

Above the photosphere, the second layer of solar atmosphere is known as chromosphere which is 2500 km thick and begins from temperature minimum region as shown in Figure

1.2. The thickness of chromosphere varies along horizontal scales. In the chromosphere temperature rises from temperature minimum (4300 K) to 10^4 K (Priest, 2014). The complex behavior of chromosphere is highly dominated by waves and oscillations. Acoustic waves generated in convection zone dominate in internetwork lanes with 3 min period (Carlsson, 2007; Hansteen *et al.*, 2006).

The bright magnetic network of chromosphere is associated with strong magnetic flux tubes at the supergranular boundaries in the photosphere. This spatial correlation of magnetic field elements in different layers of the Sun is due to the presence of large scale magnetic flux tubes ($\approx kG$) in the photosphere (Solanki, Inhester and Schüssler, 2006). The chromospheric magnetic field elements are brighter and larger than photospheric elements, and they are associated with the super-granular cells and related magnetic network elements (cf., Figure 1.5).

The high magnetic fields of the sunspots and bright plage regions also show their appearances in the chromosphere in the solar active regions (cf., Figure 1.5). The solar chromosphere consists of spectacular magnetic structures and plasma dynamics at diverse spatio-temporal scales (e.g., a variety of cool jets, solar prominence and filaments, etc). This demonstrates that chromosphere is a very dynamic layer of the solar atmosphere that plays an important role in energy and mass transport processes (e.g., waves, shocks, flows/jets, small/large–scale reconnection etc).

Transition Region

Solar transition region is optically thin layer between the chromosphere and corona. This thin layer of the solar atmosphere has $\approx$ 100 km thickness and in this region temperature increases from 0.02 MK to 0.8 MK. Transition region behaves like a bridge between large temperature gradient of chromosphere ($\approx$ 0.01 MK) and corona ($\approx$ 1 MK) and acts like a separating layer between high dense chromospheric plasma ($n \approx 10^{16} m^{-3}$) and less dense coronal plasma ($n \approx 10^{12} m^{-3}$). The transition region plays a significant role

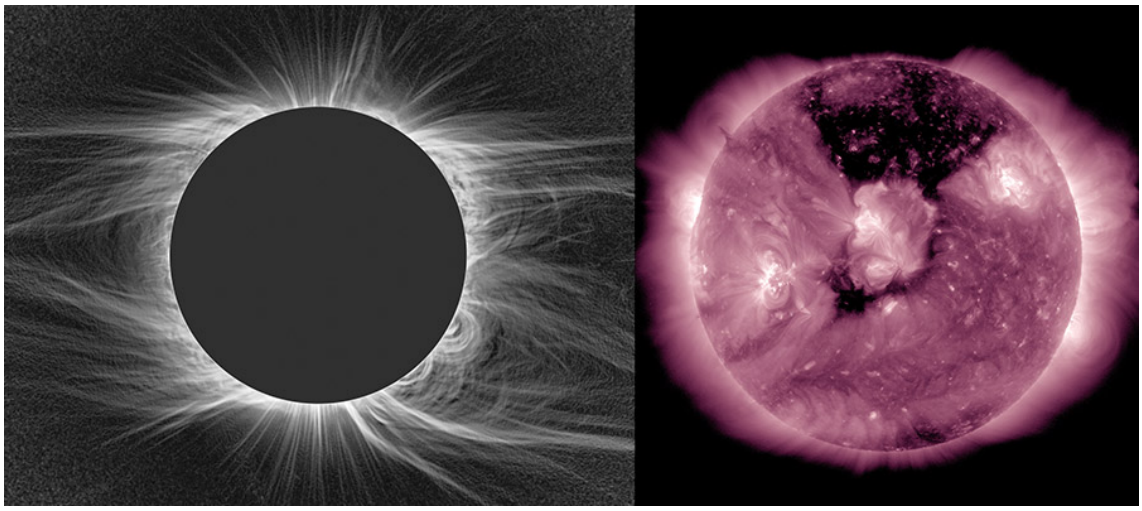

Figure 1.6: Two views of the Sun's corona, i.e., during an eclipse (left) and in ultraviolet emissions from SDO/AIA 211 Å (right) (Courtesy: NCAR High Altitude Observatory and NASA SDO/AIA)

in transportation of plasma as well as energy in the quiet Sun and active Sun e.g., solar eruptions (Mariska, 1992).

The transition region mostly emits radiation in extreme ultraviolet (EUV) and far ultraviolet (FUV) spectral wavelengths (400 Å - 1600 Å) e.g., C IV, O IV, Si IV ion lines which are observed by different space-based observatories such as Interface Region Imaging Spectrograph (IRIS), Solar and Heliospheric Observatory (SOHO) and Transition Region and Coronal Explorer (TRACE).

Corona

The corona is observed at the time of solar eclipse as bright and halo ring of less density and high temperature ($\approx$ few MK; left-panel of Figure 1.6). The diffuse corona is visible due to the Thomson scattering of photospheric light (Aschwanden, Poland and Rabin, 2001). There are different kinds of corona observed as K-corona (generated by scattering of photospheric light with electrons and their polarized continuum emission spectrum), L-corona (emission lines of highly ionized atoms), F-corona (absorption line

spectra of photospheric Fraunhofer lines). K-corona dominates within the 2.3 $R_{\odot}$ region where electron number density is $10^{14}m^{-3}$ (Aschwanden, 2004).

The dynamic behavior of corona is highly dominated by magnetic field. The Solar corona can be distinguished in different magnetic field configurations e.g., quiet Sun, active regions and coronal holes (right panel of Figure 1.6). Corona has much higher temperature (1-2 MK) than chromosphere or photosphere (Figures 1.3). Densities are lower than those of chromosphere or photosphere. It is pervaded by a magnetic field strength of $\approx$1 mT, mostly in the form of loop structures. Temperature, density, and magnetic field strength are much enhanced over sunspot regions ("active regions"). Reduced density and temperature and open magnetic fields at poles, particularly at solar minimum are coronal holes. Corona undergoes an 11-year activity cycle like photosphere and chromosphere which is brighter and more irregular at solar maximum.

1.4 The Solar Magnetic Field: A Source of Solar Transients

Magnetic field in the Sun works as an agent which couples solar interior to different layers of the solar atmosphere. The complex magnetic field is responsible factor for a variety of solar transient phenomena, e.g., eruptive prominences, solar flares, coronal jets, CMEs, flows and heating of the solar atmosphere (e.g., Forbes, 2000; Priest and Forbes, 2002; Shibata and Magara, 2011; Wiegelmann, Thalmann and Solanki, 2014). The Sun's magnetic field is generated in tachocline region (i.e., region lies between radiative and convection zone) by solar dynamo process and exhibits the formation of bright points, sunspots and faculae at the solar photosphere and then it releases in the outer solar atmosphere, heliosphere and also links the interplanetary space (e.g., Garaud, 2002; Hood and Hughes, 2011; Parker, 1970; Rudiger and Kitchatinov, 1997; Solanki, Inhester and

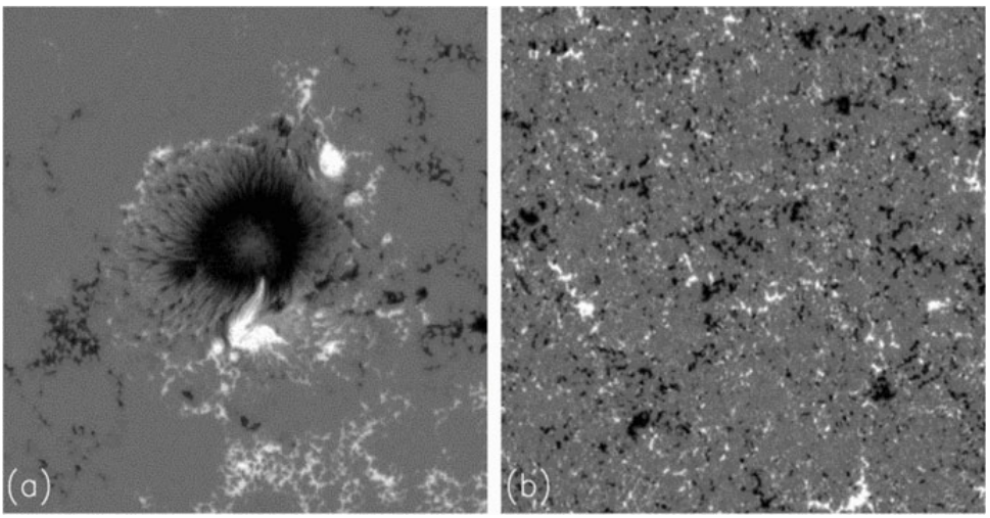

Figure 1.7: Image of a large sunspot in the left panel and quiet Sun in the right panel taken by Spectro-Polarimeter of the Solar Optical Telescope (SOT) onboard Hinode. (Courtesy: Parnell *et al.* (2009))

Schüssler, 2006). The dynamo process generates toroidal (azimuthal component) magnetic fields which emerge as bipolar regions at solar photosphere and forms coronal loops. Root of these coronal loops lies on sunspots or faculae regions (Priest, 2014; Spruit, 2002). The photospheric magnetic field is concentrated in bundles of field lines (flux tubes) which covers $\approx 5\%$ of total solar surface and field strength of these flux tubes about $\approx 1-2$ kG (e.g., Jafarzadeh *et al.*, 2014; Solanki, 1993; Spruit, 1976; Steiner, 2007). Magnetic field applies Lorentz force on all charged particles (electrons and ions) in solar regions by which all charged particles move in gyromotion along field lines. If kinetic energy of the charged particles is higher than magnetic energy then in this condition these charged particles can diffuse into the magnetic field (Aschwanden, 2004). These two different mechanisms (gyromotion of charged particles along field lines and diffusion of charged particles in the magnetic field) can be distinguished by plasma β parameter which is the ratio of thermal pressure p_{th} and magnetic pressure p_m (Gary, 2001).

$$\beta = \frac{p_{th}}{p_m} = \frac{2\mu_0 p}{B^2} \tag{1.14}$$

Plasma β parameter is about 0.2-0.4 at the solar surface when we consider gas pressure within the flux tube. Below the solar surface it increases with the depth and attains value of 10^5 at the convection zone and in coronal regions it is $\beta \ll 1$ (Solanki, Inhester and Schüssler, 2006). In coronal regions when plasma β is very low then coronal magnetic field retains its force free arrangement.

Solar magnetic field is observed by using Zeeman effect and best observation of Zeeman effect is found in photospheric spectral lines (Aschwanden, 2004; Dulk and McLean, 1978; Stenflo, 2001). The line-of-sight magnetic field is calculated by Zeeman-Doppler shift which is observed in photospheric spectral lines (Kramar, Inhester and Solanki, 2006; Semel, 1989). The Zeeman Effect of Sun is the splitting of solar spectral lines in the presence of the magnetic field. The magnetic field at the solar surface is measured by Zeeman effect because Zeeman effect is very well observed in solar photospheric spectral lines due to appropriately strong magnetic field present there. There are many instruments such as Solar Optical Telescope (SOT) (Tsuneta *et al.*, 2008) onboard HINODE (Kosugi *et al.*, 2007), Michelson Doppler Imager (MDI) (Scherrer *et al.*, 1995) onboard Solar and Heliospheric Observatory (SOHO) (Domingo, Fleck and Poland, 1995), Helioseismic and Magnetic Imager (HMI) (Scherrer *et al.*, 2012) onboard Solar Dynamics Observatory (SDO) (Pesnell, Thompson and Chamberlin, 2012) which observe photospheric magnetic field behavior. The sunspot groups in the active region possess intense magnetic field of the order of 1000 Gauss (cf., left panel of Figure 1.7) from where the coronal loops (strongly magnetized fluxtubes) fanout into the corona (cf., Figure 1.6).

The quiet Sun magnetic field is well characterized above the photosphere and in the chromosphere with a demonstration of the supergranular boundary as an appearance of the magnetic network. These networks are constituted by the bright multiple magnetic flux elements. The interior of the supergranular cell represents as the internetwork in the solar chromosphere where weaker magnetic fields are present. The internetwork field is

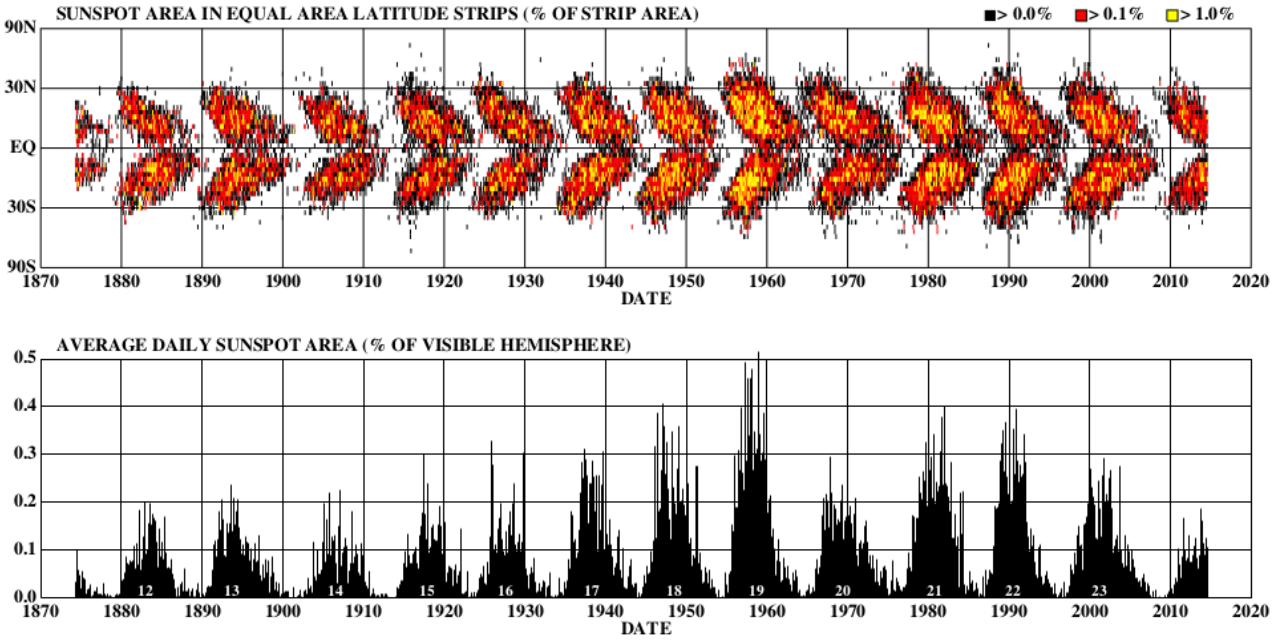

Figure 1.8: Upper panel shows sunspot area with latitude and time. Sunspots form in group, one in northern hemisphere and another in southern hemisphere and their formation starts at 25° latitude from equator. Bottom panel shows averaging of daily sunspot area as function of time. (Courtesy: Hathaway (2015))

a mixed polarity region having magnetic flux strength of 100–300 G. It is situated in the supergranule interior. The strongly magnetized and localized bright points are also seen in the magnetic networks as an intense magnetic elements of few kilo-Gauss (cf., right-panel of Figure 1.7). Overall the large-scale magnetism of the Sun's surface is governed by the 11-year solar cycle, which is described below in the next sub-section.

1.4.1 Solar Cycle

Solar activity has 11-year cycle (Hathaway, 2015). Sunspots are dark and cool patches on the solar surface which have high magnetic fields and generally these regions are the primary physical measurements of the solar activity (Babcock, 1961; Wittmann and Xu, 1987). At the initial phase of the solar cycle, majority magnetic fluxes lie in positive and negative polarity regions (i.e., sunspot groups) (Cowling, 1975). The newly emerged

bipolar regions (active regions) lie in east-west rotational direction (Stenflo and Kosovichev, 2012; Tlatov, Vasil'eva and Pevtsov, 2010). Large bipolar regions are newly emerged regions from solar interior while unipolar fields are found in solar polar regions and indicate decaying phase of the active regions (Wiegelmann, Thalmann and Solanki, 2014). We do not emphasize that coronal holes are formed by decaying active regions. We conjecture that in the decaying phase of active regions they look like unipolar structures. The large active regions, which contain sunspot groups, have 10^{23} Mx magnetic flux with lifetime of 30 days. The small ephemeral regions contain no sunspot groups and possess 10^{19} Mx magnetic flux with lifetime of 24 hours (Abramenko, Fisk and Yurchyshyn, 2006; Hagenaar, DeRosa and Schrijver, 2008). The ephemeral regions can be observed by magnetic field analysis (Harvey and Martin, 1973).

According to Hale's Polarity Law, in the sunspot groups (active regions), if the leading sunspot lie in northern hemisphere then it has positive polarity and following sunspot has opposite (negative) polarity and vice versa, in the southern hemisphere (Hale *et al.*, 1919). In 11-year cycle span, these sunspots change their polarity which implies that solar magnetic field has 22-year cycle (Hood and Hughes, 2011). The sunspot groups (active regions) lie within $\pm 30^{\circ}$ latitude and follow Joy's Law which states that sunspots tilt systematically where following polarity sunspot lies at higher latitude than the leading polarity sunspot (Hale *et al.*, 1919). Figure 1.8 shows behavior of sunspot area with latitude and time since May 1874. The solar activity is defined in terms of number of sunspots present at the solar surface if there is less number of sunspots it is defined as solar minimum and if number of sunspots is quite high at solar surface then it is defined as solar maximum (Hood and Hughes, 2011; Martin and Harvey, 1979). In year 1645-1715 there was no sunspot on the Sun this period is called Maunder's minimum which also known as Little Ice Age period and at this time solar activity was very low (Eddy, 1976; Spoerer and Maunder, 1890). Magnetic butterfly diagram illustrates many things such as Hale's

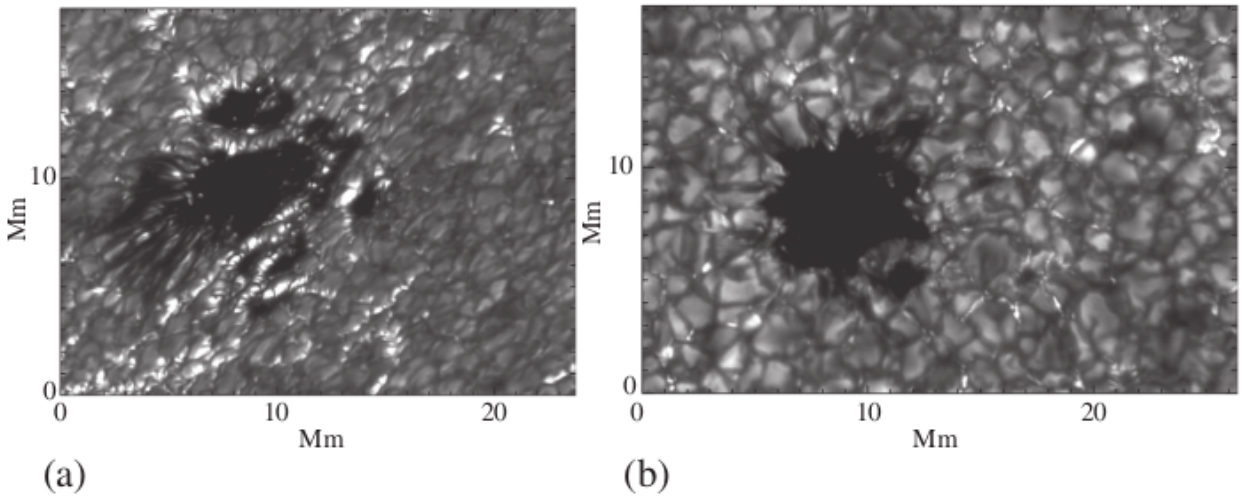

Figure 1.9: High resolution G-band observation of a faculae (left panel 'a') and bright points (right panel 'b') taken by Swedish Solar Telescope (SST) on La Palma observatory. G-band is a molecular band in the solar spectrun which is dominated at 430 nm spectral range. G-band consists electronic transitions of CH molecule in between vibrational and rotational sublevels
. Both features are found at the sides of granules and form supergranular magnetic network. These structures represent the highly localized magnetic elements in the quiet Sun. (Courtesy: Berger, Rouppe van der Voort and Löfdahl (2007))

Polarity Law, Joy's Law of active region tilt, equatorial movement of sunspot groups, behavior of overlapping solar cycles at their minimum and many other factors (Hale *et al.*, 1919; Maunder, 1903, 1904). Butterfly diagram is produced using radial magnetic fields of synoptic maps with, averaged over longitude during each solar rotation. Sunspots form in group, one in northern hemisphere and another in southern hemisphere and their formation starts at 25° latitude from equator and they migrate for high latitudes which is followed by both polarities leading as well as following (see in Figure 1.8).

1.4.2 Localized Magnetic Features on the Sun

The distribution of magnetic field at the solar surface is found in active regions and quiet Sun magnetic networks. In the active regions, magnetic flux elements are extracted in the form of sunspots and plage regions, and the plage regions are found at outside the

sunspots (Berger *et al.*, 2004; Rouppe van der Voort *et al.*, 2005; Solanki, 1993). In quiet Sun region, magnetic flux makes network elements at the boundary of supergranular cells and internetwork elements in between the supergranular cells (Solanki, 1989; Title, Tarbell and Topka, 1987). The network elements have size of 20-40 Mm and 3×10^{18} Mx magnetic flux (Solanki, Inhester and Schüssler, 2006). Magnetic features e.g., faculae, network and internetwork are anchored in the downflowing plasma in granulation process of convection zone (Title, Tarbell and Topka, 1987). Pores are dark structures having 1000 km diameter and if we compare sunspots with pores it can be concluded that magnetic pores look like a sunspot which has no penumbral region and these regions have intense magnetic flux concentration (Keppens, 2000). The magnetic elements in active region as well as quiet Sun are concentrated in high magnetic flux regions which are separated by low magnetic flux regions. Figure 1.9 shows faculae and bright points observed by Swedish Solar Telescope (SST) at La Palma observatory.

1.4.3 Relation of Magnetic Field with Dynamic and Transient Phenomena

The coronal magnetic field is evolved dynamically in small scales to very large scales where in small scale events, magnetic field is rearranged by magnetic reconnection process and in large scale events global magnetic field is recycled. SDO/AIA high temporal and spatial coronal data gives us the opportunity of detailed study of coronal dynamics in recent times. Force free magnetic modelling can also interpret coronal dynamics. For studying the coronal field evolution there are two methods, first is force-free extrapolation and another is magnetic flux transport model (Aschwanden, 2004). The reconfiguration of twisted and line-tied magnetic field of active regions contribute in the energization of coronal plasma and heated energy is released in the form of different eruptions e.g., solar flares, coronal jets, prominences and CMEs (Archontis and Török, 2008; Hood and Hughes, 2011;

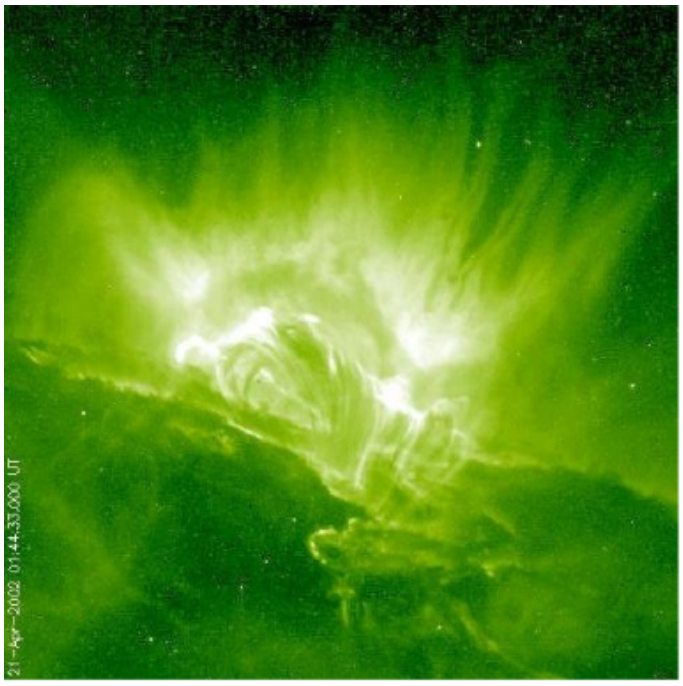

Figure 1.10: A solar flare is observed on 21 April 2002 by TRACE satellite in 195 Å filter (Fe XII). Impulsive and decaying phases of the flare is noted together. An irregular brightening pattern is observed in an impulsive phase of the flare. The post flare loops are also expanding that shows the evolution of the decaying phase of observed solar flare. (Courtesy: Benz (2008))

Manchester *et al.*, 2004; Shibata *et al.*, 1992; Shibata and Magara, 2011). The detailed observational and numerical study of these eruptive events provide us proper and clear understanding of magnetic fields structuring of eruption and expansion of magnetic fields from photospheric to coronal regions.

1.5 Transient Phenomena in the Solar Atmosphere

The Sun's atmosphere exhibits a variety of the transient and eruptive phenomena and diverse spatio-temporal scales. A few major such phenomena are described below.

1.5.1 Solar Flares

Solar flares are observed across the whole electromagnetic spectrum from radio to the gamma ray emissions (e.g., Benz, 2008; Fletcher *et al.*, 2011; Hurford *et al.*, 2003, 2006; Krucker *et al.*, 2011; Schrijver *et al.*, 2006). In general, the magnetic reconnection is responsible process for triggering of solar flares. This phenomenon may reconfigure the coronal magnetic fields and release the magnetic energy in the form of heat and kinetic energy (e.g., Carmichael, 1964; Hirayama, 1974; Kopp and Pneuman, 1976; Shibata, 1999; Sturrock, 1966). Magnetic reconnection is a process through which highly stressed magnetic fields can relax and release energy to the local plasma through the reconnection of field lines (Shibata, 1999). High energy flares are observed in active regions only. Small flares or confined flares and network flares may occur in quiet Sun. However, the large size typical flares are primarily associated with the δ-configured complex active regions in the solar corona (Benz and Krucker, 1998; Berghmans, Clette and Moses, 1998; Régnier and Canfield, 2006). The emitted heat in flares can energize and accelerate coronal loops from 1.5 MK to 30 MK temperature. Figure 1.10 shows an example of solar flare eruption observed by TRACE satellite in 195 Å filter. The flare emission is not solely a coronal phenomenon because corona and chromosphere act as a conjoint medium for the eruption of a solar flare, and range of physical processes are associated with it in different regions of the solar atmosphere. The solar flares can be classified in different classes according to their emitted soft X-ray (SXR) flux in 1-8 Å wavelength range which is calibrated by *Geostationary Orbiting Environmental Satellites* (GOES). Different classes of flares are A ($10^{-8}\ Wm^{-2}$), B ($10^{-7}\ Wm^{-2}$), C ($10^{-6}\ Wm^{-2}$), M ($10^{-5}\ Wm^{-2}$), and X ($10^{-4}\ Wm^{-2}$), which are in the ascending order of the emitted X-ray flux (Hannah *et al.*, 2011; Krucker *et al.*, 2011).

The flare goes through different phases in its whole duration of eruption as preflare phase, impulsive phase, flash phase and decay phase (Benz, 2008). In the preflare phase,

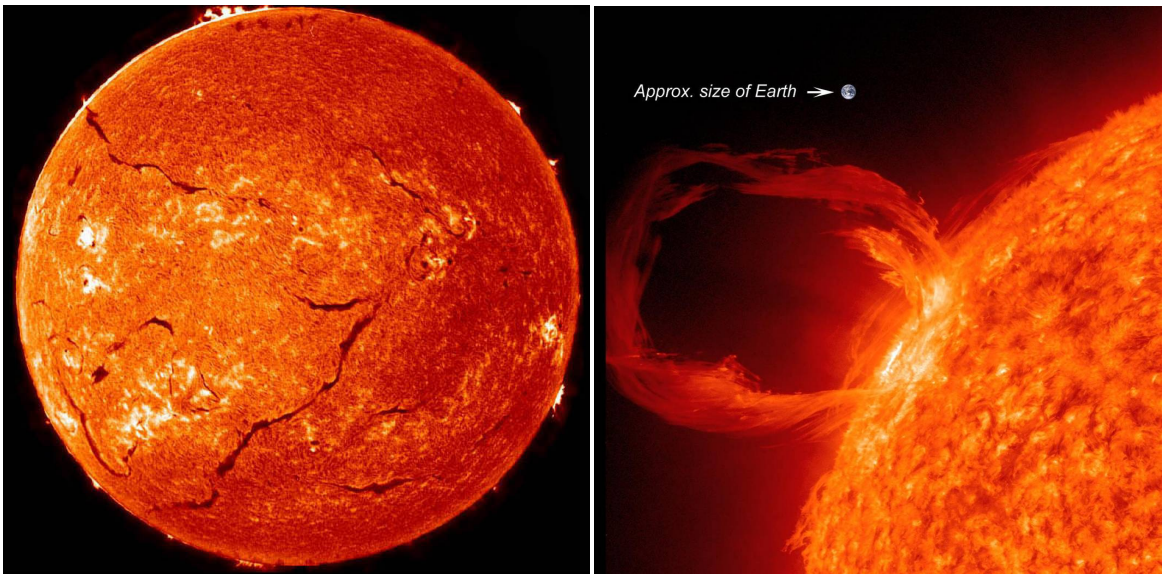

Figure 1.11: Left panel shows the solar chromosphere where dark thin filaments are well observed. Right Panel shows a solar prominence observed on March 30, 2010 in EUV wavelength. The size of the Earth is also denoted in the image to compare with the size of the prominence. (Courtesy: https://aasnova.org/2019/04/17/exploring-filaments-on-the-sun/)

flaring coronal plasma slowly energizes which is quite observable in EUV and soft X-ray wavelength bands. In the impulsive phase, a large number of electrons, ions get energized, which further release huge amount of energy and in this phase the hard X-ray footpoints at chromospheric height is also visible (Hoyng *et al.*, 1981). After attaining the impulsive phase, the chromospheric and soft X-ray emissions reach at there highest values. The quick increment in the chromospheric intensities and observed spectral line widths from the flaring region signify the flash phase of the solar flare. In the decay phase of the flare, the flaring coronal plasma returns back to its ground state with some exceptions e.g., shock waves and magnetic reconnection, energization of the electrons and ions are constantly in the higher coronal region which tend to drive radio bursts and other interplanetary processes there, evolution of post flare loop systems, etc.

1.5.2 Solar Filaments and Prominences

The solar prominences are chromospheric phenomena which are best visible in $H\alpha$ and Ca II K lines. They appear as dark, thin, multi-threaded filament structures when observed on solar disk. When they are observed off the solar limb, they look like a bright cloud and known as a prominence structure (e.g., Hirayama, 1985; Labrosse *et al.*, 2010; Mackay *et al.*, 2010; Tandberg-Hanssen, 1995; Zirker, 1989). Figure 1.11 shows the dark thin filaments on-disk in the solar chromosphere and a large prominence off the limb. Generally filaments lie along a polarity inversion line (PIL) where radial magnetic field changes its polarity (Chae *et al.*, 2001; Gibson and Fan, 2006; Pneuman, 1983; Priest, Hood and Anzer, 1989). Polarity Inversion line seperates positive and negative magnetic polarities at the solar photosphere, So it can be defined at the solar photosphere. Solar filaments are the bundle of vertical threads which move with the velocity of $10\,\mathrm{km\,s^{-1}}$ (Gouttebroze, 2008; Gunár *et al.*, 2008). Filaments consist of three-part structures, which are spine, barbs and legs of the filament (Lin, Martin and Engvold, 2008). Filaments are classified in two types according to their chirality of the filament channel (i.e., the chromospheric region which surrounds the polarity inversion line where filament resides). One is sinistral and the second is dextral filament channel. The chirality of the filament channel is described by the direction of axial magnetic field observed by an observer on positive polarity side of the polarity inversion line (PIL). If axial magnetic field moves to the right then this is a dextral type filament channel. When the axial magnetic field moves towards the left then it is known as a sinistral type filament channel (e.g., Leroy, Bommier and Sahal-Brechot, 1983; Martin, Marquette and Bilimoria, 1992; Martin, Bilimoria and Tracadas, 1994; van Ballegooijen, Priest and Mackay, 2000; Zirker *et al.*, 1997). The filaments are basically formed from the evolution of an arcade along a PIL where the magnetic field topology traps chromospheric material. There are different types of filaments according to their location of evolution and underlying magnetic field characteristics e.g., polar

crown filaments, active region filaments and quiescent filaments (Mackay *et al.*, 2010). Sometimes, filaments fade away instantly and follow an accompanied physical phenomena where the filament eruption is associated with the underlying chromospheric brightening and increased/decreased soft X-ray emissions (Schmieder *et al.*, 2000).

Quiescent prominences are more stable than other prominence. Active prominences have short duration life times and these are very dynamic which are usually found in the active regions. The average physical parameters of a typical well grown prominence may be, *viz.*, temperature 7000 K, length 200 Mm and width 5 Mm (Berger *et al.*, 2008; Engvold *et al.*, 1990). However, these parameters, especially the length and width of the solar prominence, may vary over a wider span of the length-scale. The prominence chromospheric plasma ($\approx 6 \times 10^3 - 10^4$ K) expands vertically which is surrounded by hot coronal plasma ($\approx 10^6$ K) (Labrosse *et al.*, 2010). The prominences are anchored from below the chromosphere at the boundary of a supergranular cell. There are some models to study prominence stability in the coronal surrounding as Kippenhahn-Schlüter (K-S) (1957) model (Heinzel and Anzer, 1999; Kippenhahn and Schlüter, 1957) and Kuperus & Raadu (K-R) (1974) model (Kuperus and Raadu, 1974). According to K-S model prominence plasma is supported by solar gravity and horizontal component of the magnetic field is tilted by prominence mass. The current associated with the horizontal field acts in the transverse direction and Lorentz force balances the prominence mass. The current bent original magnetic field and the whole structure of filament is balanced by magnetic tension of the bent field. According to K-R model the filamentary material is condensed with a current sheet. The gravity of the filament plasma is in static equilibrium with the vertical gradient of the magnetic tension.

As discussed above, a solar prominence may be in the stable configuration if the magnetic pressure and mass of the prominence remain in the stable equilibrium. However, once this balance is disturbed, the solar prominence may undergo in the eruptive phase

(Archontis and Hood, 2013; Aulanier, DeVore and Antiochos, 2002; Karpen and Antiochos, 2008). There are likely physical situations which can disturb the stability of a prominence and makes it eruptive, e.g., flux emergence and evolution of a new magnetic field structure, etc. A prominence might erupt as part of a CME which is destabilized by the evolution of new magnetic field and subsequent reconnection process (Gilbert *et al.*, 2000; Gopalswamy *et al.*, 2004). Generally, the helically braided and twisted flux tubes are found in the magnetic flux rope structure of a prominence where eruptions of flare and CME are quite observable as the resultant products (Jing *et al.*, 2004). In the next sub-section, we will emphasize on understanding the properties of another localized transients, which are termed as "Coronal Jets". They are sometimes associated with the mini-filament or partial filament eruptions, and the CMEs. The present thesis basically describe some new scientific results related to the coronal jets and their association with the CMEs/narrow-CMEs.

1.5.3 Coronal Jets: An Observational Understanding

Coronal jets were first observed by UV telescope of US Naval Research Laboratory (NRL) in 1980's and after that they were observed by Soft X-ray Telescope (SXT) of Yohkoh Japanese spacecraft in early 1990s (Shibata *et al.*, 1992; Strong *et al.*, 1992). Solar coronal jets are the narrow plasma beams. There are many small scale explosive and jet-like events in the solar atmosphere (e.g., from nanoflares or microflares to explosive events, blinkers, jets, etc) that all display small-scale signatures of processes that are associated with flares and, indeed, some believe that some of these phenomena could be regarded a small-scale flares at the low-energy end of a flare spectrum. Coronal jets are magnetically driven phenomena and have straight or twisted structures. The height of the jets is found to be 1×10^5 km and their width is smaller than their height ranging from $2 \times 10^2 - 2 \times 10^4$ km and lifetime is 100-2500 s (e.g., Cirtain *et al.*, 2007; Raouafi *et al.*, 2016; Shimojo *et al.*, 1996; Shimojo, Shibata, and Harvey, 1998; Shimojo and Shibata, 2000). According to the

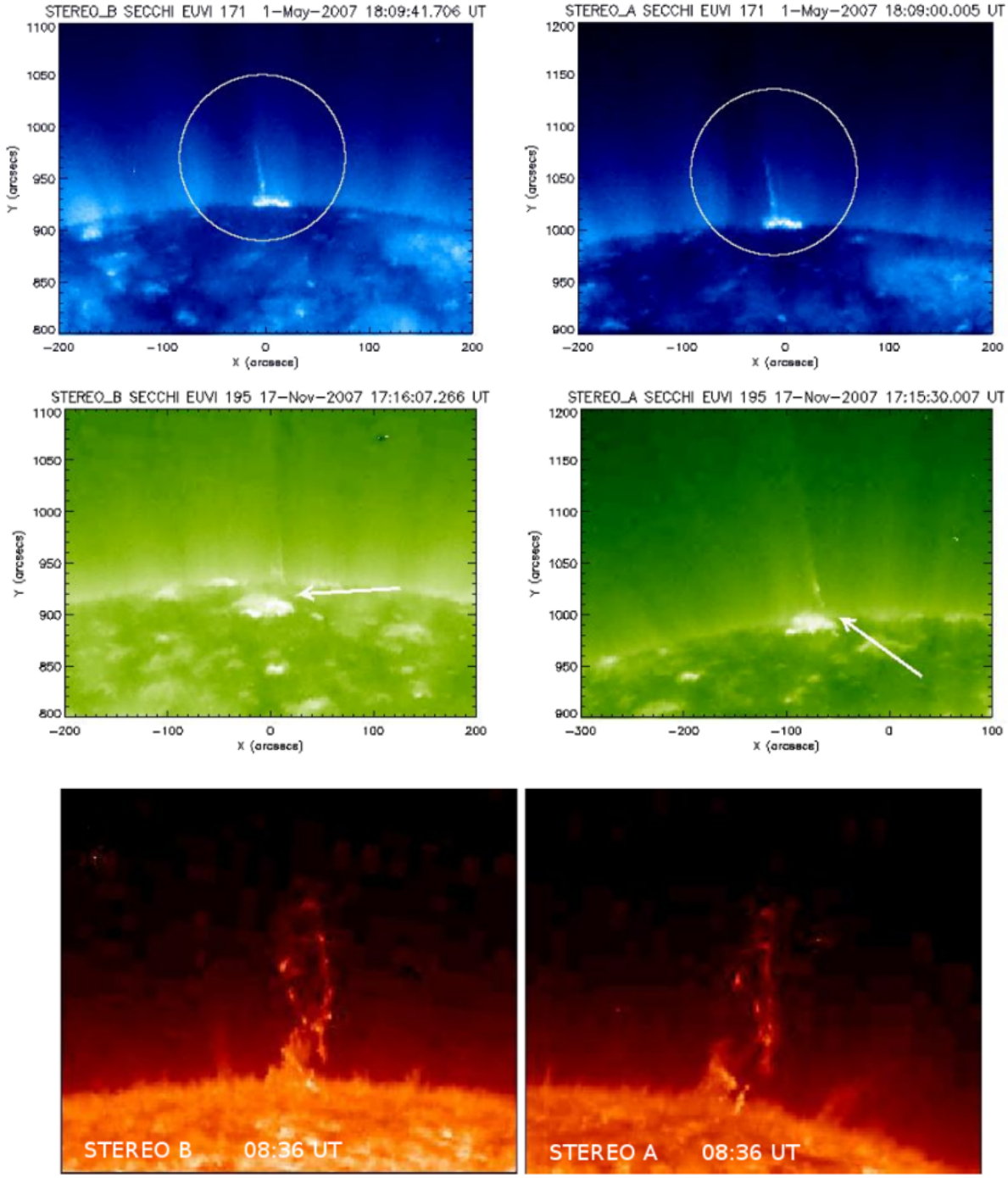

Figure 1.12: Upper panel shows an Eiffel tower jet observation in EUVI 171 Å filter of STEREO_A and STEREO_B. Middle panel shows λ-shaped jet in 195 Å filter of STEREO_A and STEREO_B. Bottom panel shows a helical jet on 08 February 2008 in EUVI 304Å filter of STEREO_A and STEREO_B. (Courtesy: Nisticò *et al.* (2009))

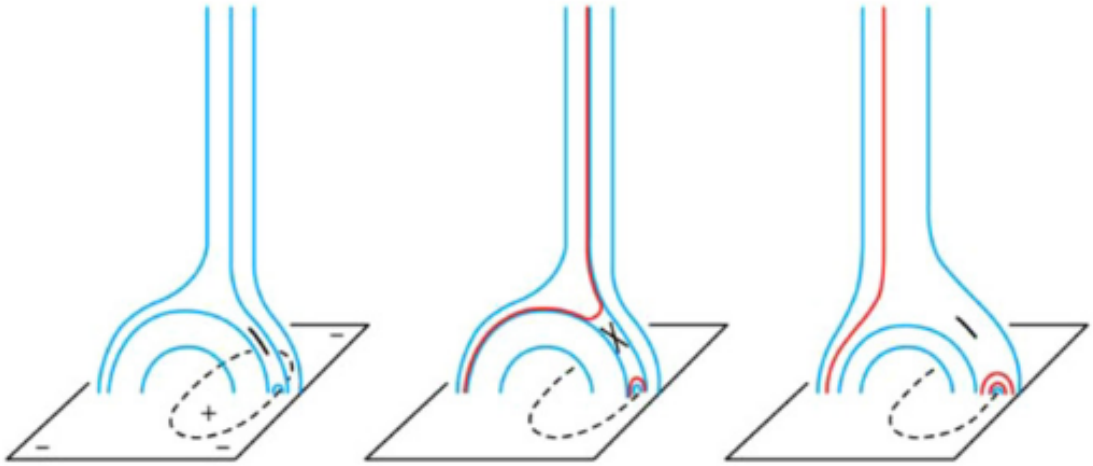

Figure 1.13: Cartoons represent the standard model of the coronal jet eruption. Left cartoon shows an initial field configuration. Black dashed line represents a polarity inversion line. Middle cartoon shows a slanted current sheet formation where burst of reconnection occurs and jet is erupted along the red newly reconnected lines. Right cartoon shows the decaying phase of the jet eruption. (Courtesy: Moore *et al.* (2010))

Hinode observations, flows along jet eruption show two kinds of velocities one is Alfvénic ($800\,\mathrm{km\,s^{-1}}$) and another is magneto-acoustic velocity ($200\,\mathrm{km\,s^{-1}}$) (Cirtain *et al.*, 2007). Usually jets occur in all solar regions e.g., active region, quiet Sun and coronal holes but their appearance is more prominent in coronal holes due to its darker surrounding. Recent improvements in spatial and temporal resolution of different imaging and spectroscopic data of space based observatories e.g., Yohkoh, SOHO, STEREO, Hinode, SDO, IRIS provide finer details about morphology, evolution and dynamics of coronal jets. The solar minimum and solar maximum conditions affect the evolution of coronal jets as at the solar maximum coronal jets are more massive and brighter than at the solar minimum (Wang and Sheeley, 2002).

Nisticò *et al.* (2009) have done statistical study of coronal jets in polar and equatorial coronal hole regions taking SECCHI/EUVI and COR1 observations. According to this study, coronal jets can be characterized in different classes as Eiffel tower jets and λ-shaped jets. This study also suggests that Extreme Ultra-violet (EUV) jets show helical structures.

Figure 1.12 shows Eiffel tower, λ-shaped jet and helical jet observations in different EUV filters of STEREO_A and STEREO_B. They have analyzed 79 polar jets where 37 show Eiffel tower shape (inverted-Y shape), 12 show λ-shape and 5 jets are micro-CME type. In all the observed jets, 31 jets show helical structures and possess torsional motion along their propagation axis. In Eiffel tower jets, the bipolar field reconnects with the open coronal field at the top of its loop and in λ-shaped jets, the bipolar field reconnects with the open coronal field at its footpoints. Micro-CME jets are identified by presence of small loops which extend from solar surface and look like smaller CMEs.

A contradiction/difference of solar X-ray jets between the standard reconnection scenario and non-standard reconnection scenario (blow-out eruption) is reported by Moore *et al.* (2010, 2013) in XRT/Hinode observations. Figure 1.13 shows cartoons of standard model (Shibata *et al.*, 1992) for coronal jet eruption. Moore *et al.* (2010) observed solar X-ray jets in coronal holes and found that 67 % of the observed jets follow standard reconnection scenario (i.e., standard jets) of Shibata *et al.* (1982, 1992, 2007) while 33 % follow non-standard reconnection scenario (i.e., blow-out jets). These non-standard jets are blow-out jets which are correlated with erupting $H\alpha$ macrospicules. In blow-out jets, the sheared and twisted base arch undergoes a miniature blow-out eruption which also drive CMEs. Figure 1.14 shows model of blow-out jet eruption and blow-out jet observation by X-ray Telescope (XRT) onboard Hinode. The different numerical simulations and observational results indicate that most of the coronal hole jets are blow-out jets (e.g., Adams *et al.*, 2014; Archontis and Hood, 2013; Panesar, Sterling and Moore, 2018; Pariat *et al.*, 2015; Sterling *et al.*, 2015; Wyper, DeVore and Antiochos, 2018). Sterling, Moore and DeForest (2010) have also reported that there are large number of spicules (type-II spicules) which possess chromospheric blow-out jets behavior.

Sterling *et al.* (2015) have done observational study of coronal hole X-ray jets and found some discrepancies in jet productions which are incompatible with emerging flux

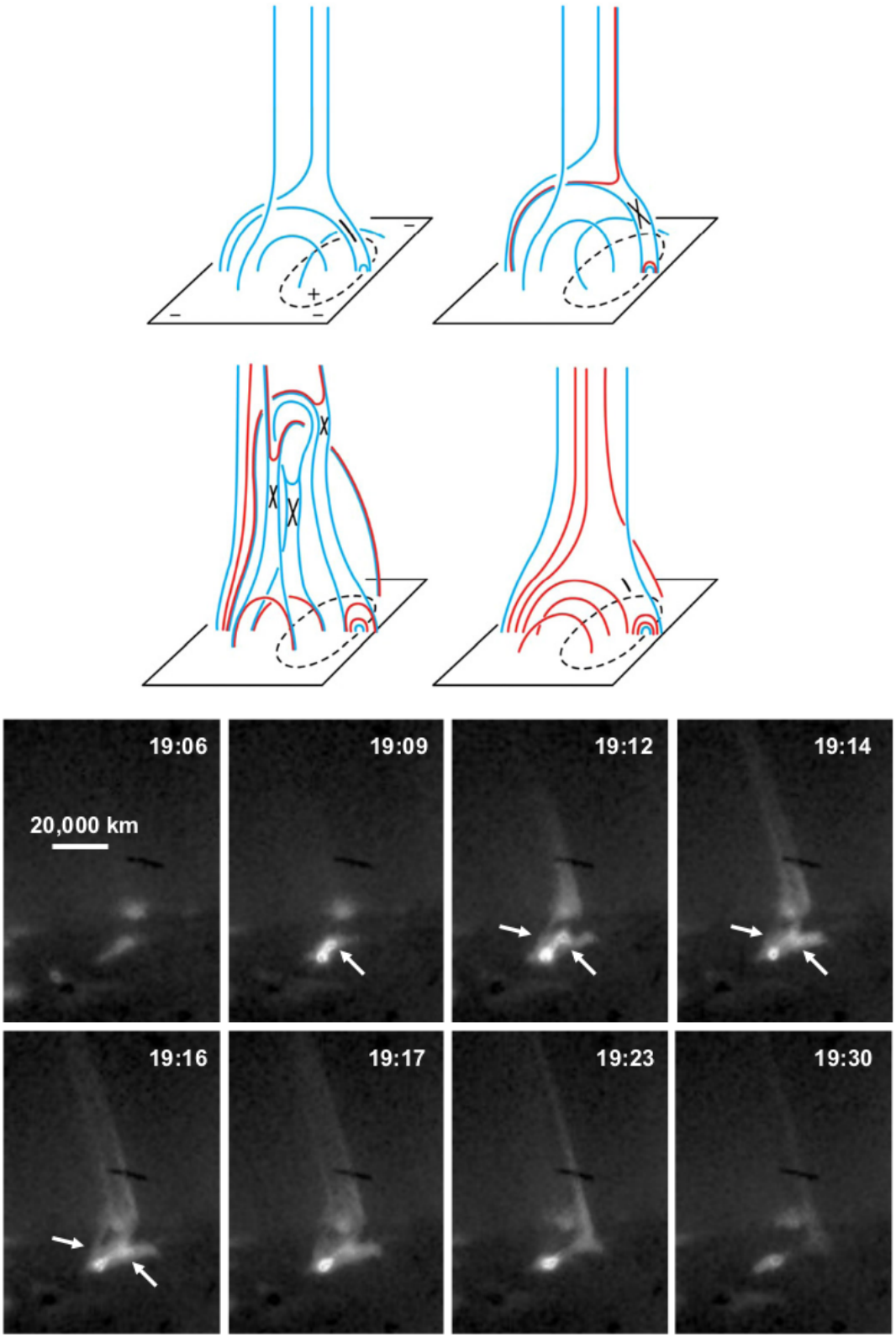

Figure 1.14: In upper panel cartoons represent model for blow-out jet eruption. Red lines are newly reconnected magnetic field lines. Base arch field is stronly sheared which reconnect with open field and initiate blow-out eruption. Bottom panel shows blow-out jet observed on 20 September 2008 by X-ray Telescope (XRT) onboard Hinode. (Courtesy: Moore *et al.* (2010))

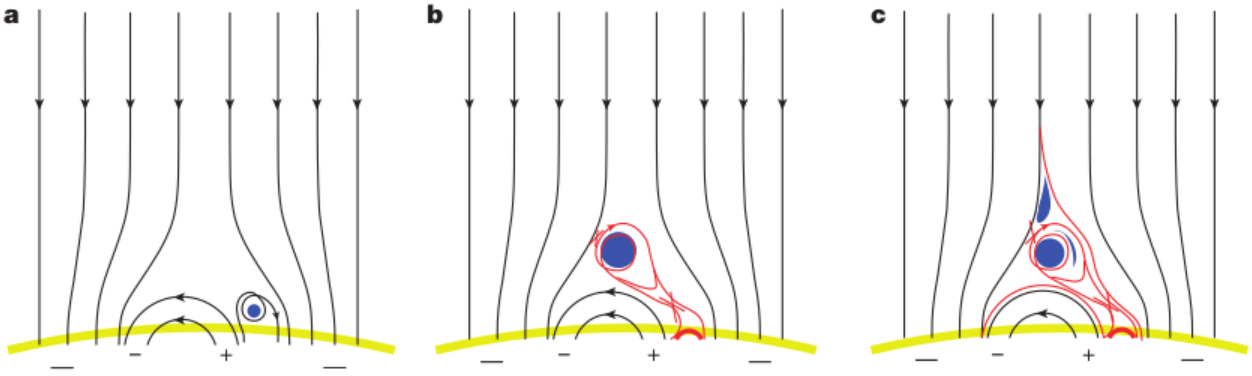

Figure 1.15: Revised model of jet eruption based on mini-filament eruption process. In this figure, yellow line represents the solar limb, blue feature is mini-filament material and red lines are newly reconnected magnetic field lines. Panels (a), (b) and (c) represent different states of mini-filament driven jet eruption. (Courtesy: Sterling *et al.* (2015))

model of (Shibata *et al.*, 1989). Sterling *et al.* (2015) have proposed mini-filament eruption model for generation of the coronal jets. Figure 1.15 shows mini-filament eruption model of coronal jet eruption. In this model, eruption of mini-filament induces jet producing magnetic reconnection. This model supports that filament eruption is a universal magnetic process which can take place in broad solar scales and drives flares, coronal jets and CMEs according to their sizes and scales. Internal reconnection in terms of magnetic flux cancellation and emergence gives rise to mini-filament eruption that create jet bright point (i.e., JBP) and when this mini-filamentary field goes through external reconnection it generates newly reconnected open magnetic field lines which drift away successively to drive coronal jets. Sterling *et al.* (2015) have also re-defined the standard jet and blow-out jet generation process in their model as if mini-filaments fully erupt from base regions then they will drive blow-out jets and if mini-filaments show confined erupting behavior and do not get away from base region then they will drive standard jets. In the present thesis, we have also presented a novel example of the multiple jet eruptions due to the eruption of the mini filaments, which were associated with the quiet-Sun supergranular cell and also with the network flaring events.

In the lower solar atmosphere (e.g., chromosphere, transition region) very dynamic small jet-like activities, e.g solar surges, spicules, plumes and network jets are also observed which play an important role in supplying of mass and energy to coronal regions (De Pontieu *et al.*, 2011). Solar surges are cooler counter-parts of the coronal jets observed in chromospheric $H\alpha$ lines. Surges have height of 2×10^5 km, lifetime of $10-20$ min and they move with apparent speed of 50-200 $\mathrm{km\,s^{-1}}$ (Chen *et al.*, 2006; Kuridze *et al.*, 2011; Schmieder, Golub and Antiochos, 1994). Sometimes, these surges are associated with Ellerman bomb brightening in intense magnetic fields (Reid *et al.*, 2015, 2016; Roy, 1973). There are many factors which drive these surges e.g., flux emergence, cancellation, magnetic reconnection and impulsive pressure pulses (Gaizauskas, 1996; Kayshap, Srivastava and Murawski, 2013; Shibata *et al.*, 1982; Sterling, 2000). Bong, Cho and Yurchyshyn (2014) studied dynamics of recurrent active region chromospheric surges using Solar Optical Telescope (SOT) onboard Hinode observations and found rotational signature of surges. Chromospheric $H\alpha$ surges are correlated with EUV and X-ray eruptions on same spatial scales (e.g., Canfield *et al.*, 1996; Schmieder *et al.*, 1988; Schmahl, 1981; Shibata *et al.*, 1982; Svestka, Farnik and Tang, 1990).

1.5.4 Coronal Jets: The Perspective of the Numerical Models

Shibata, Nozawa and Matsumoto (1992) have performed 2-D numerical simulations to examine the magnetic reconnection process between overlying coronal field and emerging magnetic field. For this study, they used 2-D emerging flux model of Shibata *et al.* (1989, 1990) and in this model a constant gravitational acceleration in negative z-direction is also considered. At the time of reconnection between emerging and overlying coronal field, the chromospheric plasma goes down to the loops and forms a jet bright point (JBP). The eruption of soft X-ray jets and $H\alpha$ surges is observed at near to current sheet. The multiple magnetic islands are found in current sheet which evolved at Alfvén speed and the cool,

high-dense chromospheric plasma are confined in these islands. By extending this model, Kayshap, Srivastava and Murawski (2013) have re-produced the observed large-scale cool jet (e.g., surge-like structure) due to chromospheric heating. They have devised a numerical model with conceivable implementation of the VAL-C atmosphere and a thermal pulse as an initial trigger. VAL-C is a classical model of the gravitationally stratified solar atmosphere which defines solar plasma properties upto 3 Mm height which comprises upper photosphere, chromosphere, transition region and the lower coronal region. This model studies perturbations and wave propagation in the solar atmosphere. They found that the pulse steepens into a slow shock at higher altitudes which triggers plasma perturbations exhibiting the observed features of the surge-like cool large-scale jet (cf., Figure 1.16).

Yokoyama and Shibata (1995, 1996) have also performed the resistive 2-D MHD numerical simulations based on emerging flux and magnetic reconnection process for two types of jets (i) Anemone and (ii) two-sided loop jet. Two-sided loop jets are the pair of horizontal jets which have loop-like structure. These are produced by emerging magnetic flux in quiet regions and horizontal coronal fields are present there. While the Anemone jets are vertical in nature. They are also produced by magnetic flux emergence in coronal hole regions and vertical coronal fields are present there. The kinetic energy (1.2×10^{28} ergs) and velocity ($100\,\mathrm{km\,s^{-1}}$) of these jets were calculated and their values are found in good agreement with the observed solar X-ray jets. The hot and cool jets ($H\alpha$ surges) found simultaneously in this model which also suggests the co-existence of solar X-ray jets and $H\alpha$ surges. This numerical model is not found realistic because there are many computational limitations in the model and this could not produce self-consistent jet and emerging flux. This numerical model is performed at low temp (0.25 MK) and high density ($10^{12}\ cm^{-3}$) for the solar coronal regions which is quite unrealistic. The Alfvén velocity is also found lower compared to its exact value in the model. Nishizuka *et al.* (2008) have numerically modelled the jet formation (inverted Y-shaped jet) observed in NOAA AR

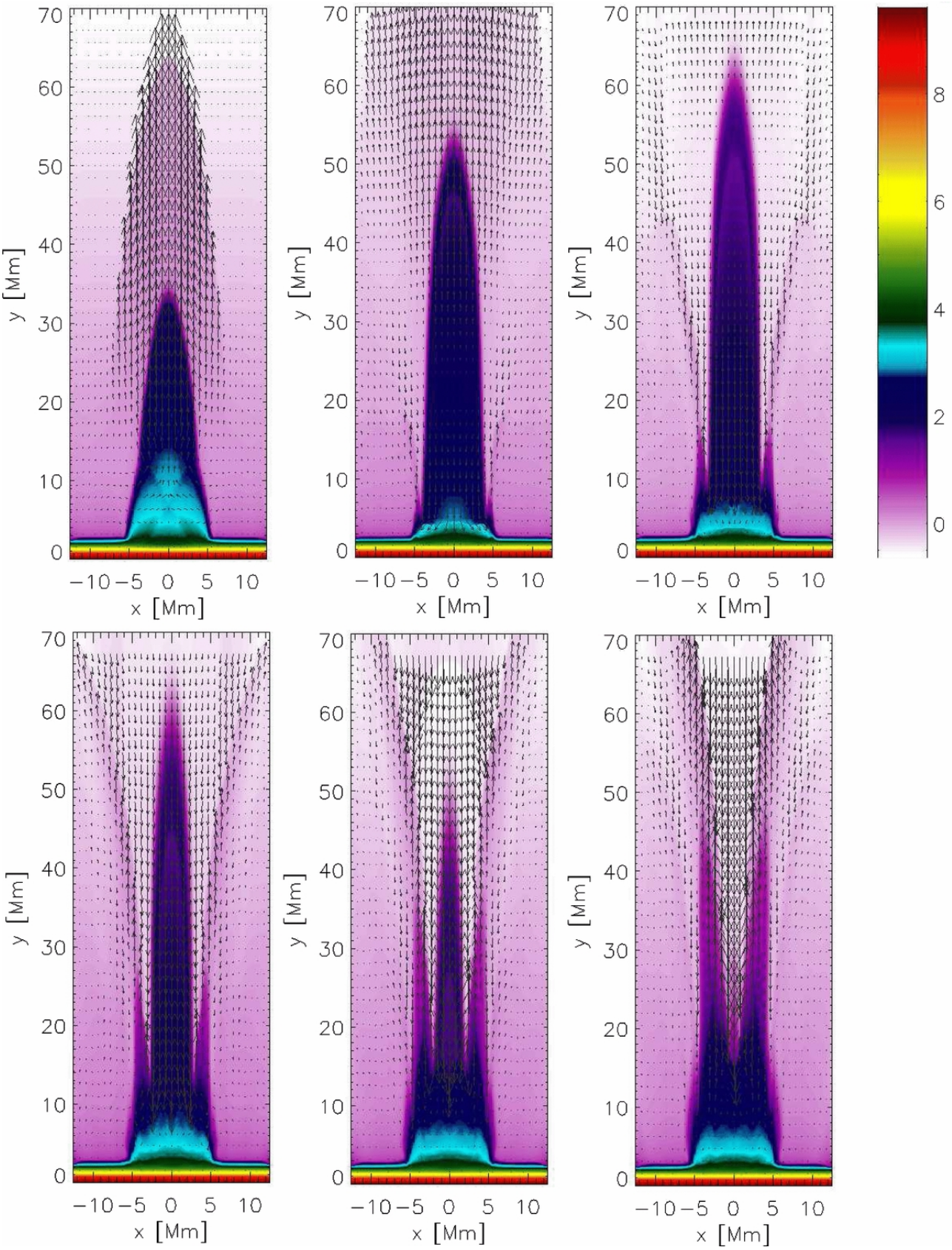

Figure 1.16: Temporal snapshots of a simulated thermal pulse driven cool jet. The density (color maps) profiles at t = 200 s, t = 400 s, t = 600 s, t = 800 s, t = 1000 s, and t = 1200 s (from top to bottom). Density is drawn in the units of 10^{-12} kg m^{-3} as shown in the color bar, which is common to all the panels. The velocity vector unit is 150 km s^{-1}. (Courtesy: P. Kayshap)

10940 on the west solar limb on 2007 February, 9 at 13:20 UT in a more realistic way. They had improved 2-D MHD computational approach taken higher temperature (10^6 K) and lower density (10^{10} cm^{-3}) for the coronal regions. This was the first numerical model which was able to reproduce self-consistent emerging flux and jet. In this model, thermal conduction and radiative cooling effects were not taken into account so the jet formation was solely a magnetic activity which did not depend on the gas pressure. In this model, the reproduction of co-existing hot and cool jets and generation of propagating Alfvén waves have been done successfully. This model supports the reconnection model of Yokoyama and Shibata (1995, 1996).

Heggland, De Pontieu and Hansteen (2007) numerically simulated 1-D MHD model of jet formation due to shock waves in the solar upper regions. Monochromatic piston was used as a driver at chromospheric boundary to generate acoustic oscillations. In this model velocity and deceleration of jet were simulated which are dependent on amplitude of initial disturbance, inclination angle of field and period. The simulated quantities were found in good agreement with observations and also found good correlation between velocity and deceleration. Heggland, De Pontieu and Hansteen (2009) numerically simulated jet-like activity using 2-D MHD of wave-induced magnetic reconnection model in chromopshere and transition region where the radiative loss and heat conduction were taken into account. In this model, the monochromatic piston was used as a driver for periodic reconnection. This results give basic understanding of different jet-like activities e.g., explosive events, spicules and blinkers phenomena.

In another study, Heggland *et al.* (2011) successfully simulated the jet formation and propagation of waves in the solar atmosphere with 2-D Bifrost code taking different parameters e.g., radiative losses, thermal conduction, magnetic diffusion, different magnetic field structures and their different inclination angle into account. In this model, it was noticed that inclined magnetic field had more impact on propagation of long period waves

rather than radiative relaxation time. The jet activity had different features in inclined and vertical fields. The velocity signals of waves in strong inclined field (including edges of magnetic flux tubes) have period of 5 min but in weak or vertically oriented field velocity signals have 3 min period. These simulation results were found in good agreement with Hinode jet observations. In this model, wavelet technique was used to analysis and found that this technique was more reliable than Fourier analysis.

In proposed models for solar coronal jets the principal models are based on magnetic reconnection mechanism in typical fan-spine and null point configuration. Pariat, Antiochos and DeVore (2009) have proposed numerical model for jet activity in polar coronal hole regions. The primary goal of this model was to explain observations where short duration energy bursts lead magnetic reconnection and jets. The basic assumption of this model was that the magnetic reconnection is not allowed in axisymmetric null-point configuration till some magnetic stress/instability breaks the symmetry of this magnetic field configuration. Once this symmetry is destroyed huge energy released via magnetic reconnection in form of massive jets. Pariat, Antiochos and DeVore (2010) numerically modelled the eruption of successive quasi-homologous jets. Continuous magnetic stress at photospheric surface was applied to produce homologous jets. The homology of jets was maintained by null-point configuration which tend to relax in its initial state. Archontis and Hood (2013) reported 3-D numerical simulations of standard and blow-out jets and their trasition behavior based on magnetic flux emergence and reconnection process. The external reconnection between emerging and overlying field generates standard jets while the internal reconnection of sheared emerging flux generates flux rope and blow-out jet eruption.

Pariat *et al.* (2015, 2016) have done parametric study of solar coronal jets by 3-D numerical modelling using ARMS numerical solver. In this model, the effects of different parameters e.g., field inclination, plasma β and field distribution on formation of standard and blow-out jets was studied. The surrounded magnetic field impacts the triggering and

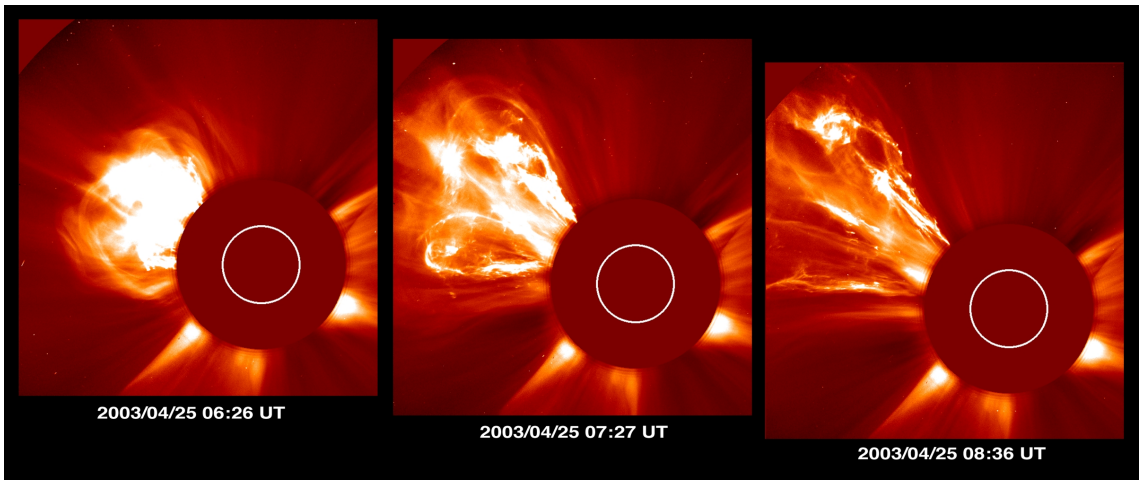

Figure 1.17: A giant CME is observed on 25 April 2003 by Large Angle Spectroscopic Coronagraph (LASCO) C2 coronagraph. The evolution period of this CME is about 2 hours where strong expansion of cloud is observed. (Courtesy: https://sohowww.nascom.nasa.gov/gallery/images/trioc2.html)
.

energization of different jets. Wyper, Antiochos and DeVore (2017); Wyper, DeVore and Antiochos (2018) have proposed magnetic breakout reconnection model for eruption of mini-filament directed coronal jets. According to this model, twisting jets were formed when mini-filament became unstable and erupted. The formation of jets were dependent on the inclination angle of background magnetic field and its strength. There were different phases of eruption in this model first highly sheared mini-filament channel was formed, second this filament was lifted up (i.e., erupting flux rope) and undergone to breakout reconnection, third a twisting blow-out jet was formed via breakout reconnection and in fourth phase this whole configuration was relaxed.

1.5.5 Coronal Mass Ejection

CMEs shoot out a huge amount of plasma and magnetic fields into the heliosphere. These eruptions can produce interplanetary shocks, energetic particles events and affect the space-weather conditions on the Earth (e.g., Low, 2001; Webb and Howard, 2012; Zhang

and Low, 2005). Figure 1.17 shows a CME eruption on 25 April 2003 observed by Large Angle Spectroscopic Coronagraph (LASCO) C2 coronagraph. CMEs are accompanied with various phenomena like flares, eruptive prominence, coronal jets, EUV waves, type II and type IV radio bursts and coronal shocks. LASCO C2-Large Angle Spectroscopic Coronagraph (LASCO) C2 is a coronagraph onboard Solar and Heliospheric Observatory (SOHO). This is white light coronagraph which observes 1.5-6 solar radii regions. EUV waves- Extreme-Ultraviolet (EUV) waves are propagating bright fronts observed in extreme ultraviolet filters. This phenomena is firstly observed by Extreme-Ultraviolet Imaging Telescope (EIT) onboard Solar and Heliospheric Observatory (SOHO) in 1998. Type II radio bursts - Solar Type II radio bursts are first reported in 1947 by Payne-Scott and these bursts are stimulated by magnetohydrodynamics (MHD) shocks in the solar atmosphere. These are the narrow frequency bands in radio spectra. Sometimes, these bursts are accompanied with solar flares and CMEs. Type IV radio bursts- These are complex radio bursts. These are continuum emissions at metric and decimetric wavelengths in the radio spectra. Type-IV bursts are often associated with CMEs. CMEs have different forms, e.g., classical structure (three part structure:- compressed bright plasma front, dark cavity and bright filamentary core), narrow jets, streamer blowouts and halo CMEs. The released mass in CME eruption is about $10^{15} - 10^{16}$ gm, kinetic energy is about 10^{31} ergs and frontal part of CME has a speed of $20\,\mathrm{km\,s^{-1}}$ - $2000\,\mathrm{km\,s^{-1}}$ (e.g., Gosling *et al.*, 1976; Howard *et al.*, 1985; Hundhausen, Burkepile and St. Cyr, 1994; Low, 2001; St. Cyr *et al.*, 1999, 2000; Webb and Howard, 2012). A large magnetic structure achieves a situation that lacks equilibrium or reaches an instability, and it erupts-this can be driven by emerging or merging fields, and processes such as reconnection, in a variety of magnetic configuration (Low, 2001; Zhang and Low, 2005).

1.6 Motivation and Brief Outline of the Thesis

The field of solar eruptive phenomena is very vast. In the last 20 years, a considerable development in the observational and theoretical understanding of coronal jets was perceived. These ejecta play an important role in solar activities and coronal heating as well as mass supply. The study of jet associated CMEs is also an important subject these days. Jet associated CMEs can affect Earth's magnetosphere and space weather conditions may also arise. Recent space-based solar observatories (e.g., SDO, Hinode, STEREO) give us the opportunity to refine our understanding of coronal jets and their relationship with CMEs/narrow-CMEs. This thesis aims to understand the different properties of coronal jets and their formation mechanisms, as well as to explain relationship between coronal jets and CMEs. We also study the role of mini-filaments in the formation of some coronal jets, and explored their linkage with narrow CMEs.

Hong *et al.* (2011) reported first observation of a quiet Sun blowout jet triggered by mini-filament and associated with a micro-CME. These results give insight that mini-filaments have same properties as large-filaments where large-filaments drive massive CMEs and mini-filaments drive mini-CMEs. Shen *et al.* (2012) reported first observation of twin-CMEs (bubble-like CME and jet-like CME) with a quiet Sun blow-out jet. Bubble-like CME is associated with cool component of blow-out jet and jet-like CME is associated with hot component of blow-out jet. Based on their observation they proposed twin-CME model which elucidate that external reconnection causes lifting of mini-filament, jet-like CME and internal reconnection causes bubble-like CME.

Adams *et al.* (2014) reported eruption of an EUV macrospicule in coronal hole region driven by a mini-filament eruption. The flux cancellation and converging flow at base of macrospicule makes mini-filament arcade unstable which goes through blow-out eruption and generate macrospicule. Sterling *et al.* (2015) reported observations of solar X-ray jets in polar coronal hole region. The miniature version of mini-filaments drive these

solar X-ray jets. Li *et al.* (2015) observed active region blow-out jet which triggered by mini-filament eruption. This jet eruption is accompanied with a eruptive M-class flare which further evolve in form of CME. Li *et al.* (2017) observed a blowout surge caused by interaction and successive reconnection between small scale filaments and large scale coronal loops. Hong *et al.* (2017) observed two co-spatial jets in active region in these jets, first jet shows typical fan-spine configuration while second jet is full blow-out jet. In case of first jet, mini-filament is confined in magnetic fields but in case of blowout jet mini-filament fully erupts. This blow-out jet is associated with C-1.6 solar flare and type-III radio bursts.

Panesar *et al.* (2016) observed quiet Sun coronal jets and found that each quiet region jet is driven by mini-filament eruption. The continuous magnetic flux cancellation triggers mini-filament eruption which further drag jets. Panesar, Sterling and Moore (2018) observed coronal hole jets and found that mini-filament plays important role in eruption of coronal hole jets. The magnetic flux cancellation is responsible mechanism for coronal hole jet eruptions. Sterling *et al.* (2016, 2017) observed active region coronal jets which are driven by mini-filaments and continuous flux cancellation is responsible process for these eruptions.

In my research I have carried forward the observational works of coronal jets in this direction as what is the role of mini-filaments in eruption of coronal jets. What is relation and association of coronal jets with CMEs? What are the conditions when a coronal jet becomes CME-productive and non-productive? Although the above questions are answered through the specific original scientific research, in general, we study the fundamental physical processes in a solar atmosphere and the ubiquitous observation of jets clearly points to a common process in terms of magnetic field / plasma interaction, particle acceleration processes etc in the present thesis. That occur all over the atmosphere and that we feel therefore that research into jets is potentially extremely important In this

thesis, we have focused on coronal jets observations and their relationship with coronal mass ejections. The study of coronal jets provides critical and significant knowledge about the bigger and more complex drivers of the solar activity. The study of the solar eruptions and CMEs and their forecast in causing space-weather is a potentially important tool for solar and heliospheric research.

Chapter 2 outlines the space and ground-based observatories and their instruments, which were utilized to observe the specific coronal jets and associated dynamics (e.g., surge eruption, network flare, CMEs, K-H instability, etc) studied in the present thesis. This chapter also describes a variety of analysis techniques, e.g., image calibration and alignments; analysis of magnetograms and coronagraphic data; magnetic field extrapolation technique; Fourier Local Correlation Technique to measure the photospheric optical flows, Tie-pointing method to measure the kinematics of jets in STEREO triangular observations, etc.

Chapter 3 of the present thesis provides first detailed observations and inter-relationship between quiet-Sun network-flare, eruption of multiple segments of filaments, episodic formation of coronal jets, and evolution and propagation of two CMEs in the outer corona. The twin CMEs as jet-like and bubble-like CMEs have been observed by LASCO-C2 onboard the SOHO and STEREO-A and STEREO-B/COR2, which are associated with the eruption of northern and southern sections of the filament and formation of blowout jet eruptions.

Chapter 4 provides the details of the study of recurring jets near active region AR11176 during the period 31 March 2011 17:00 UT to 01 April 2011 05:00 UT using observations from SDO/AIA. Two Mini-filaments were found at the base of these recurring jets where the first mini-filament is found at the base of first three jets showing its partial eruption. The second mini-filament at the base of fourth jet shows complete eruption and drives evolution of a full blow-out jet. Second mini-filament also triggers a C-class, GOES C-3.1,

flare and full blow-out jet. This blow-out jet further triggers a CME. The plasma blobs are detected during the eruption of first jet. The continuous magnetic flux cancellation is found at the base of jet productive region which is the reason of eruption of mini-filaments and recurring jets. The presented scientific result provides a new scientific information on the linkage of mini-filament eruptions with the multiple coronal jets, and differentiate about the CME-productive and non-productive jets.

Chapter 5 provides the information about the observational study of a complex active region jet which evolved from southward of a major sunspot of NOAA AR12178 on 04 October 2014. This complex jet is associated with a GOES C-1.4 flare and a cool surge. We have termed this jet as a two-stage confined eruption. In first stage of jet, some plasma erupts above the compact flaring region and in second stage eruptive jet plasma and associated magnetic fields interact with another set of magnetic fields in south-east direction. At the interaction point of these two different magnetic fields a null point (X-point) is created, where second stage of jet deflected along curvilinear path into overlying corona. The magnetic flux cancellation at the base of jet causes a C-class flare and the flare energy energizes first stage of coronal jet. The lower part of jet is followed by a cool surge visible only in Hα emissions. This two-stage jet observation imposes some rigid constraints on existing jet models as described in details in subsection 1.5.4

Chapter 6 describes the conclusions of all the presented works in this thesis. It also provides some details of the future plan on the emerging research field on the study of coronal jets and their relation with the CME eruptions.